RSC Advances

PAPER

View Article Online
View Journal | View Issue



Cite this: *RSC Adv.*, 2024, **14**, 9538

# Revealing the high efficiency of fluorescence quenching of rhodamine B by triangular silver nanodisks due to the inner filter effect mechanism

Tran Thu Trang,[a] Thi Thu Ha Pham,[b] Nguyen Van Dang,[a] Pham Thi Nga,[ac] Mac Van Linh[ad] and Xuan Hoa Vu *[a]

Received 23rd January 2024
Accepted 28th February 2024

DOI: 10.1039/d4ra00575a

rsc.li/rsc-advances

Performing effective fluorescence quenching based on a metal nanomaterial is essential to construct fluorescence sensors. Silver nanomaterials are well known as an excellent candidate for an absorber in fluorescence sensing systems. Herein, we investigated the fluorescence quenching of rhodamine B (RhB) in the presence of triangular silver nanodisks in which perfect overlap between the absorption of the absorber and the fluorescence of the fluorophore was observed. The fluorescence quenching mechanism of RhB was investigated under various excitation wavelengths, together with measurement of the fluorescence lifetime. The quenching efficiency of RhB was proportional to the wavelength excitation. Remarkably, the highest efficiency of fluorescence quenching of RhB was achieved (~60%). The quenching mechanism was investigated and revealed to be mostly due to the inner filter effect (IFE) mechanism, without the contribution of energy transfer. This result shows a completely different story from most previous studies based on silver nanoparticles, where energy transfer was reported to play a significant role.



## 1 Introduction

The interaction of dye molecules and metal nanoparticles is gaining popularity due to their potential application in optical sensors as well as biosensors.[1–3] Sensors based on changes in fluorescence intensity are the most commonly used because they are highly sensitive, simple, and adaptable to a wide range of analytes and systems.[2,4] One of the most powerful techniques for sensing based on changes in fluorescence intensity is fluorescence quenching.[5] Quenching is the process of reducing the intensity of an emitting molecule's fluorescence without changing its spectrum. Depending on the nature of fluorescence quenching, it could be static quenching or dynamic quenching. Fluorescence quenching due to the presence of metal nanoparticles generally occurs as a result of Förster resonance energy transfer (FRET) or nanomaterial surface energy transfer (NSET).[6,7] These fast quenching processes serve as a spectroscopic ruler to measure the intra- or intermolecular distances between interacting moieties. It has been reported that the efficiency of FRET and NEST are inversely proportional to the sixth and fourth orders of the distance between the fluorophore and absorber, respectively.[8] However, the design of such systems generally requires a complicated process. Moreover, constructing this type of fluorescence sensor with high stability in practice is often complicated and extraordinarily time-consuming.[5,9]

Together with FRET and NEST, fluorescence quenching based on the inner filter effect (IFE) mechanism is also one of the most common in the design of fluorescent sensors.[10,11] Here, IFE refers to the absorption of excitation and/or emission radiation by identical chromophores in a system.[12] In the beginning, the IFE was known as a source of errors in fluorescence measurement.[13] However, the IFE has been extensively explored for application in constructing fluorescence sensing thanks to the exponential changes in the fluorescence intensity.[14] The IFE can effectively occur when the absorption band of the absorber completely overlaps with the excitation and/or emission spectra of the fluorophore and the high optical density of samples at the excitation and emission wavelength.[15] Fluorescence sensing based on the IFE mechanism has already been exploited with different types of fluorophores from photoluminescent nanomaterials to dye molecules.[16–19]

Noble metal nanoparticles are known as excellent quenchers due to their high molar extinction coefficients and tunable absorption spectra in the visible region. The spectrum of the localized surface plasmon resonance (LSPR) is significantly dependent on a nanostructure's size, shape, dielectric constant, and the dielectric constant of the surrounding environment.[20,21] Thus, noble metal nanoparticle properties have generated much interest in optical sensing applications based on fluorescence quenching.[2,22–24] It should be noted that the high

[a]*Institute of Science and Technology, TNU-University of Sciences, Tan Thinh Ward, Thai Nguyen City, Vietnam. E-mail: hoavx@tnus.edu.vn*

[b]*Faculty of Chemistry, TNU-University of Sciences, Tan Thinh Ward, Thai Nguyen City, Vietnam*

[c]*Faculty of Secondary School, Hoa Lu University, 2 Xuan Thanh Street, Ninh Nhat Commune, Ninh Binh City, Vietnam*

[d]*Quang Uyen High School, Quang Hoa District, Cao Bang Province, Vietnam*

extinction coefficient of the absorber is significantly important in fluorescence quenching based on the IFE. In particular, at the same size, the extinction coefficient of silver nanoparticles is much larger than that of gold nanoparticles.[25] Therefore, silver nanoparticles are an excellent candidate for application in fluorescence quenching based on the IFE. Many studies have reported that energy transfer between noble metal nanomaterials and fluorophores plays a significant role in the fluorescence quenching of fluorophores. For example, the fluorescence quenching of coumarin,[26,27] RhB and rhodamine 6G,[3] and indopolycarbocyanine[28] in the presence of silver nanoparticles has been revealed by the FRET effect. Although these studies reported that FRET is the primary mechanism of fluorescence quenching, the specific interaction mechanism between the silver nanomaterials and dye has been shown to depend on the size and shape of the nanomaterials.[28–30]

Nonspherical nanostructures have been shown to exhibit increased LSPR sensitivities due to their sharp geometries. Triangular silver nanodisks have optical properties where the surface plasmon resonance bands are tunable throughout the visible to near-infrared regions of the spectrum by controlling the edge length, thickness, and tip morphology.[20,31,32] It has been postulated that triangular silver nanodisks could contain both dipole and quadrupole plasmon resonances, which can cause a shift in the frequency and extinction cross-section as a function of their size, shape, and dielectric surrounding environment.[33] This characteristic of plasmon resonances is different from that of spherical particles, which can not be distinguished between the two. Furthermore, triangular silver nanodisks possess a higher absorption coefficient at the excitation wavelength than that of other shapes.[31]

In this work, triangular silver nanodisks (denoted as Ag nanodisks) were used as an absorber to study the fluorescence quenching of RhB. Unexpectedly and remarkably, although the absorption of Ag nanodisks and the fluorescence of RhB presented a perfect overlap, FRET could not occur. This phenomenon was confirmed through an examination of the fluorescence lifetime of RhB with and without Ag nanodisks. Instead of the energy-transfer mechanism, the high efficiency of fluorescence quenching was clarified as the major effect, stemming from the IFE, while a minor contribution to the quenching of fluorescence stemmed from static quenching, and the highest fluorescence quenching efficiency was about 60%. This high efficiency of fluorescence quenching is consistent with the high absorption coefficient of Ag nanodisks, together with the completely overlapping spectra of the absorption spectrum of Ag nanodisks and the absorption and fluorescence spectra of RhB. This result clearly provides a simple approach for designing fluorescence quenching systems based on Ag nanodisks and fluorophores for application in fluorescence sensing.

## 2 Experimental section

### 2.1. Materials

Silver nitrate ($AgNP_3$, 99.98%) was used as the precursor of Ag. Trisodium citrate dihydrate (TSC, 99%) and sodium borohydride ($NaBH_4$, 99%) acted as reducing agents. Polyvinyl pyrrolidone (PVP) served as the stabilizer.

### 2.2. Chemical synthesis of Ag nanodisks

First, colloidal silver nanoparticle seeds (denoted as Ag NPs) were fabricated by the reduction process of $AgNO_3$ with the presence of $NaBH_4$. The synthesis of colloidal Ag NPs started with a simple aqueous phase mixing of $AgNO_3$ with TSC, PVP, and $NaBH_4$ solutions.[34] In short, a mixture of 2 ml of $AgNO_3$ (0.02 M), 400 μl TSC 0.6 M, 100 μl PVP (0.03 M), and 200 μl deionized water was prepared and magnetically stirred at room temperature for 15 min. Then, 800 μl $NaBH_4$ was dropwise added to the mixture. Finally, 200 μl of NaOH (1 M) was injected into the solution. After that, the total mixture was magnetically stirred for 15 min.

Then, to synthesize Ag nanodisks, the obtained solution above was irradiated by a green LED (light emitting diode) with a power output of ~0.5 mW $cm^{-2}$ and the LED's wavelength centered at 520 nm. Then, the absorption spectra of the mixture were examined after each interval of 10 min of green LED irradiation. The intent of the irradiation process was to turn the spherical nanoparticles into silver triangular nanodisks. This process was carried out at room temperature.

### 2.3. Absorption and fluorescence spectral studies

Mixtures of Ag nanodisks and RhB (1.2 μM) in water were prepared with different amounts of stock solutions of Ag nanodisks ($OD_{560\ nm} \sim 1.45$). The amounts of the stock Ag nanodisks were varied by 130, 200, 270, 340, 425, 495, and 565 μl in the titration mixtures with RhB (1.2 μM) in an identical total volume of 1800 μl. The absorption spectra of all samples were collected using a UV-vis spectrometer (Jasco V-770). The characteristics of fluorescence spectra and fluorescence lifetime were measured by fluorescence spectroscopy (model FLS 1000, UK). The excitation wavelengths were chosen as 349, 515, and 530 nm for the fluorescence measurements. The slit widths of the spectroscopy were kept precisely the same for all mixtures under the same excitation wavelengths. The relative fluorescence quantum yields, $\Phi_F$, were estimated using rhodamine 590 ($\Phi_F = 0.95$ in ethanol) as a reference.[35] The fluorescence lifetime decay was fitted to a single exponential decay by Igor Pro 6 with the equation: $I(t) = A \times \exp\left(-\frac{x}{t}\right)$.

### 2.4. Other instrumental techniques

The morphology of the as-prepared nanostructures was examined using an 80 kV JEOL JEM-1010 transmission electron microscopy device (TEM). The X-ray powder diffraction (XRD) spectra were obtained utilizing an X-ray diffractometer (Bruker D8 Advance, Germany) at 30 kV with Cu-$K_\alpha$ radiation (0.154056 nm) and a parallel-beam geometry ranging from 30° to 80°.

## 3 Results and discussion

### 3.1. Absorption spectroscopy study

First, absorption spectroscopy analysis was performed to determine the first sign of the changes in the Ag seeds under

green light irradiation. The optical absorption spectra and a digital photo of the Ag seeds under different time intervals of green light irradiation were recorded and are presented in Fig. 1. The color of the Ag NPs solution indicated there was a change in the color from light yellow to navy, with a simultaneous red-shift in the absorption spectrum from 400 to 573 nm. Given the connection between the nanoparticle morphology and optical properties, it follows that these characteristics can be used to assess the shape, size, and distribution of nanostructures in solution for structures with such properties. The color and absorption spectra changes have been reported as the change in size and shape of Ag seed under a shining light because of aggregation. Specifically, after 70 min of irradiation, the typical LSPR spectrum showed three peaks at around 570 nm corresponding to an in-plane dipole, at 336 nm presenting an out-of-plane quadrupole, and at 420 nm describing an in-plane quadrupole.[31,36] Then, these characteristic LSPR bands could be anticipated to form triangular silver nanodisks based on around a 100 nm-edge dimension with 10 nm snips.[20,31] In this work, the solution of Ag seeds after 70 min of shining light was used to study its effect on the fluorescence of RhB.

### 3.2. Morphology and crystal structure

To confirm the size and shape and reinforce the results of the absorption properties of the fabricated samples, the morphology and crystal structure of Ag seeds and Ag seeds after 70 min of green shining light were studied by TEM spectroscopy and XRD.

The TEM technique was implemented for the Ag seed sample and Ag seeds after 70 min of shining green light to elucidate the shape and size of the obtained samples. Fig. 2a shows the image of the Ag seeds before shining green light on them, showing that the Ag seeds were well-separated and fairly round, with a diameter of approximately 7–8 nm. This indicated there would be a good agreement between the characteristic absorption spectrum band centered at 400 nm and the round shape, together with the size being in the order of ten nanometers.[37–39] After the green light irradiation process (70 min), the Ag seeds grew into truncated triangular Ag nanodisks, with the length of each edge varying around 70–100 nm (Fig. 2b). This was in good agreement with the anticipated effects indicated by the

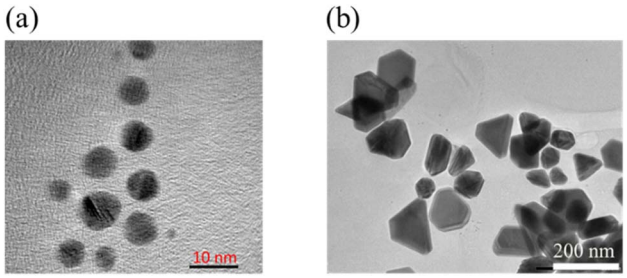


Fig. 2 TEM images of (a) Ag seeds and (b) Ag nanodisks.

characteristics of the absorption spectrum.[40] It is well known that LSPRs are formed by the coherent oscillation of conduction electrons on the surface of the nanostructure when they interact with the oscillating electric field of incident light. The frequency of this oscillation is dependent not only on the density and effective mass of the electrons but also on the size and shape of the charge distribution. Therefore, the tips of the triangular disks become rounded as the electron cloud density changes across the particular surface.[20]

The formation of Ag nanodisks could be interpreted as a result of the accumulation of tiny silver seeds *via* the Ostwald ripening mechanism under green LED irradiation.[41] This result is in agreement with previous studies using a similar green light for the irradiation process.[34,40] The XRD spectra were measured to further prove the Ag nanodisks' structural evolution (Fig. 3). In the XRD analysis results, the diffraction peaks at around 38° (111), 44.09° (200), 63.9° (220), and 76.7° (311) corresponded to the face-centered cubic structure of silver (ICCD no. 01-071-3752).[42] The high intensity peaks, without any other strange peak in the XRD patterns, proved the pure crystal structures of the silver nanostructures.

### 3.3. Study of the optical properties of RhB in the presence of Ag nanodisks

The optical properties of RhB in the presence of Ag nanodisks were investigated in comparison with those of RhB alone to clarify the effect of the Ag nanodisks on RhB, where Ag nanodisks were expected to act as a quencher.

Fig. 4a shows the absorption spectra of Ag nanodisks with different amounts of Ag nanodisks stock solution varying from

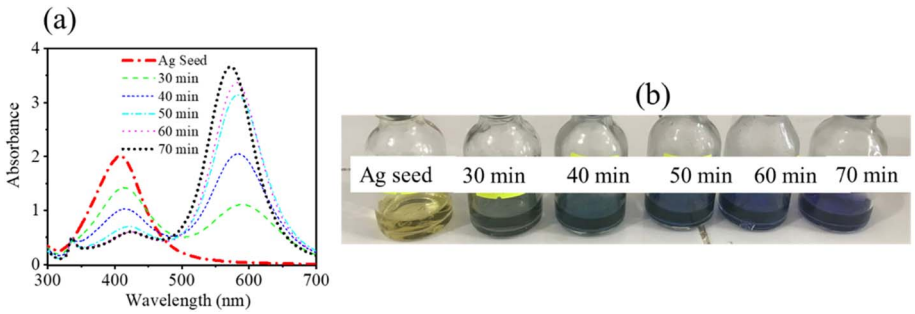


Fig. 1 (a) Absorption spectra of the Ag seeds under different time intervals of green irradiation ($\lambda_{irradiation} \sim 520$ nm). (b) Image of a digital photo of the Ag seed solution under different times of green light exposure.

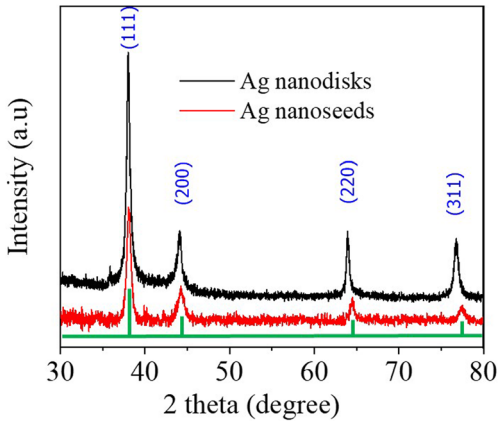


Fig. 3 XRD patterns of the Ag seeds (red line) and Ag nanodisks (black line).

130 to 565 μl. The absorption spectra of the mixing solution, including Ag nanodisks and RhB 1.2 μM, simply presented the overall absorption spectra of the Ag nanodisks and RhB. It could thus be deduced that there was no specific interaction between RhB and triangular Ag nanodisks to form a new band (Fig. 4b). This was different from the case of RhB and graphene, where the absorption spectrum of RhB revealed a decrease in intensity due to the formation of a RhB–graphene complex.[43]

To investigate the optical properties of RhB in the presence of Ag nanodisks, all the prepared samples were examined using fluorescence spectroscopy. First, the excitation spectra were measured to determine the fluorescence characteristics of the mixing solutions (Ag nanodisks + RhB) in comparison to the solution of RhB alone. The Ag nanodisks + RhB mixture in aqueous solution displayed excitation and emission characteristic bands centered at 553 and 578 nm, respectively. These characteristic bands were identical to those of RhB alone (Fig. 5). Thus, the excitation and fluorescence spectra of the mixing solution of Ag nanodisks + RhB revealed the characteristic of only the RhB component. Therefore, the fluorescence properties of the mixture solution of Ag nanodisks + RhB stemmed from only the RhB component, and we can thus ignore the possible interaction between Ag nanodisks and RhB to form a complex.

Fluorescence spectroscopy was implemented to study the optical properties of the mixture of Ag nanodisks + RhB further. The fluorescence intensities of the mixtures of Ag nanodisks + RhB and the solution of RhB alone were compared under the same conditions of measurements and are shown in Fig. 6. It is clear that the fluorescence intensity of RhB was quenched depending on the amount of Ag nanodisks. The fluorescence of RhB in the mixture solution with Ag nanodisks showed fairly strong quenching compared to the case of RhB alone. In this study, we examined the dependence of fluorescence quenching on the amount of stock Ag nanodisks and the excitation wavelength (Fig. 6a–c).

The quenching efficiencies of the mixture solution of RhB (1.2 μM) with varying amounts of Ag nanodisks were calculated using the following equation:[43]

$$\text{Quenching efficiency (QE)} = 1 - \frac{F}{F_0} \quad (1)$$

where $F$ and $F_0$ refer to the fluorescence intensity of RhB with and without the added Ag nanodisks. Fig. 6d displays the fluorescence quenching efficiency of RhB depending on the amount of Ag nanodisks stock solution as well as the excitation wavelength. The quenching efficiency (QE) of RhB seemed to be linear, increasing with the increasing amount of Ag nanodisks stock solution in the range of 130 to 425 μl. The QE at the larger amount of Ag nanodisks stock solution of 425 μl revealed though that the trend was not linear. When reaching the amount of the stock solution of Ag nanodisks at 565 μl, the fluorescence quenching was retained and reached a saturated state.

Besides examining the fluorescence intensity depending on the amount of Ag nanodisks, we evaluated the fluorescence quenching under various excitation wavelengths and the results

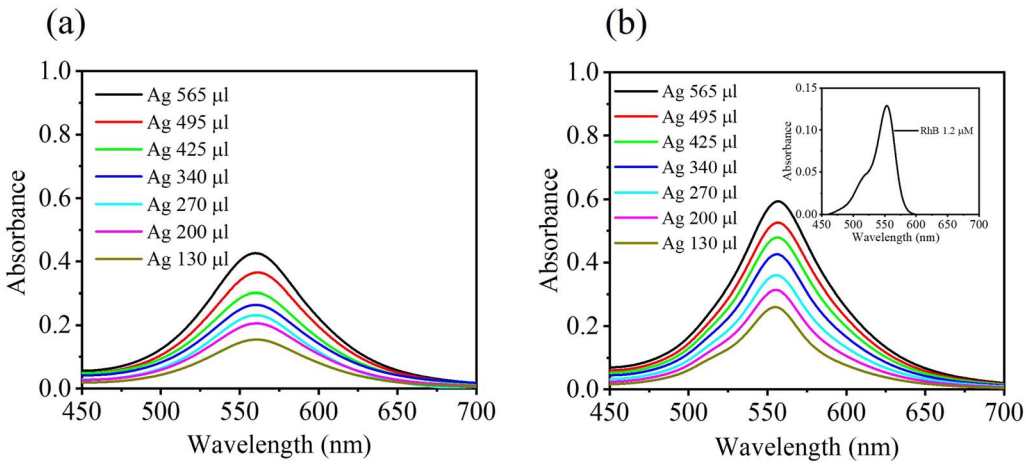


Fig. 4 UV-vis absorbance spectra for (a) varying the amounts of stock solution of Ag nanodisks from 130 μl to 565 μl in a total volume of 1700 μl; and (b) absorption spectra of mixing solutions of RhB (1.2 μM) and different amounts of Ag nanodisks. Inset figure: absorption spectrum of RhB (1.2 μM).

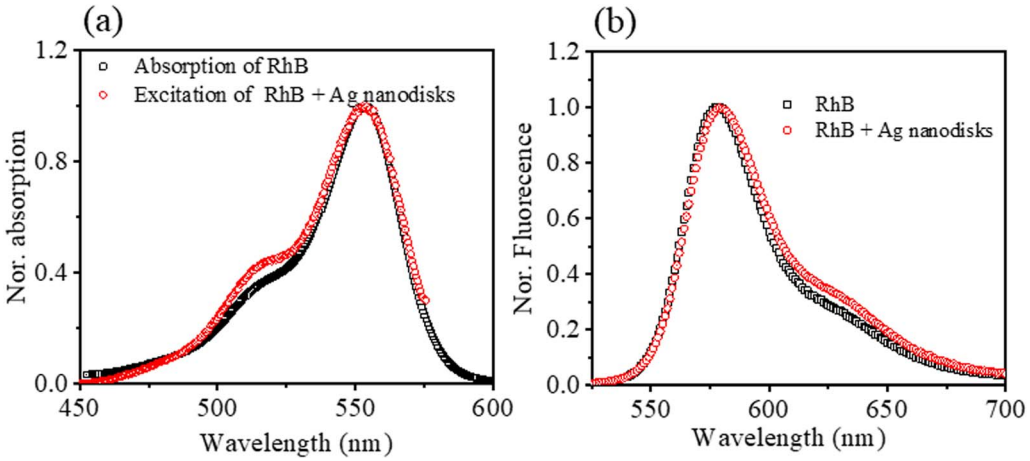


Fig. 5 (a) Normalized absorption spectrum of RhB and excitation spectrum of RhB + Ag nanodisks; and (b) normalized fluorescence spectra of RhB and mixed solution of Ag nanodisks and RhB for comparison. The samples were prepared in an aqueous solution, and the fluorescence spectra were recorded with excitation at $\lambda_{exc} = 515$ nm. The excitation spectrum was collected with monitoring at $\lambda_{em} = 570$ nm.

are presented in Fig. 6d. Three distinguished excitation wavelengths at 349, 515, and 530 nm were utilized to excite RhB in all the prepared samples to clarify the effect of excitation energy on the mixture solutions of Ag nanodisks and RhB. As seen from the absorption spectra of RhB and Ag nanodisks, the excitation wavelengths at 349, 515, and 530 nm showed an increase in the

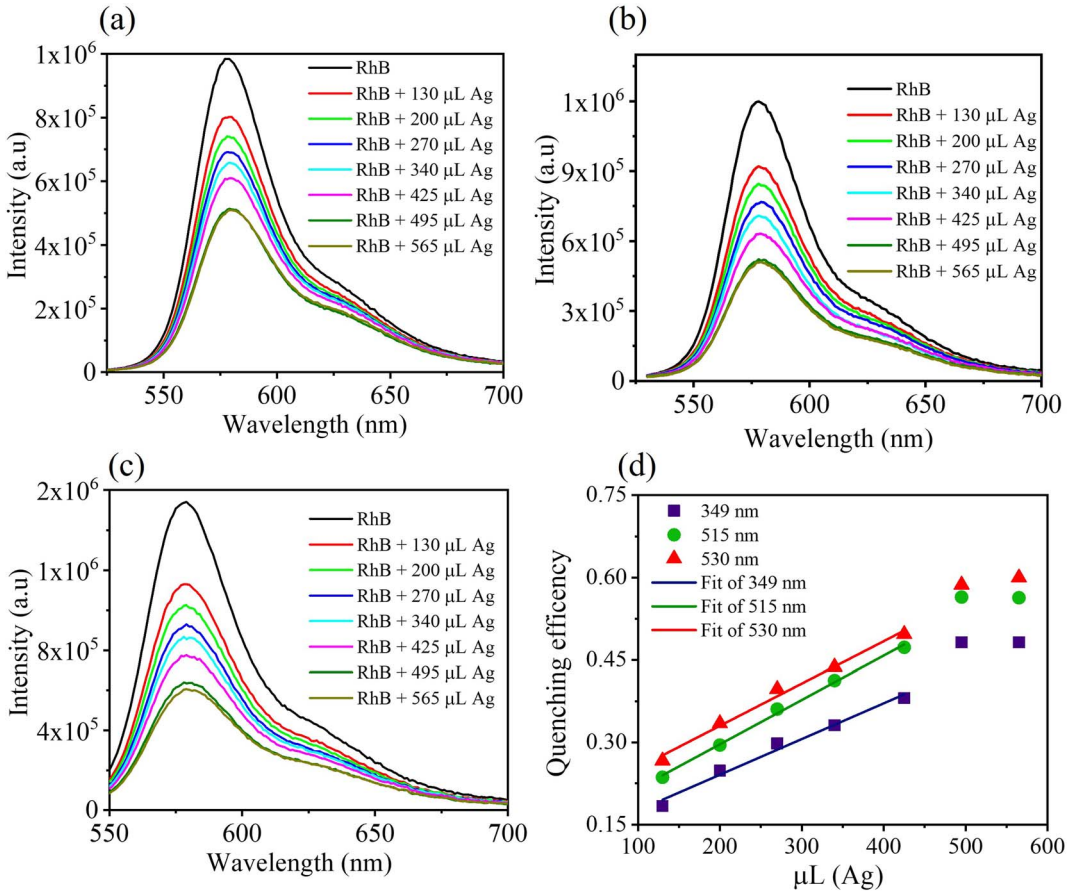


Fig. 6 Fluorescence spectra of RhB (1.2 μM) in comparison with the mixtures of Ag nanodisks + RhB (1.2 μM), with the amount of stock Ag nanodisks varying from 130 μl to 565 μl in a titration volume of 1700 μl, under different excitation wavelengths at 349 nm (a), 515 nm (b), and 530 nm (c); (d) fluorescence quenching efficiency of mixed solutions of Ag nanodisks + RhB depending on the amount of stock Ag nanodisks solution and the excitation wavelength.

Table 1 Fluorescence quantum yields of RhB with various amounts of Ag nanodisks in aqueous solution depending on the excitation wavelength; abbreviation: $\lambda_{exc}$ = excitation wavelength

| Fluorescence quantum yields ($\Phi_F$) | | | | | | | | |
|---|---|---|---|---|---|---|---|---|
| $\lambda_{exc}$ (nm) | Amount of Ag nanodisks (μl) | | | | | | | |
| | 0 | 130 | 200 | 270 | 340 | 425 | 495 | 565 |
| 349 | 0.35 | 0.30 | 0.28 | 0.27 | 0.26 | 0.24 | 0.20 | 0.20 |
| 515 | 0.35 | 0.28 | 0.26 | 0.24 | 0.22 | 0.21 | 0.17 | 0.17 |
| 530 | 0.35 | 0.27 | 0.25 | 0.23 | 0.22 | 0.20 | 0.16 | 0.16 |

absorbance of both Ag nanodisks and RhB. The QE apparently increased with the excitation wavelength and reached about 60% at the highest concentration of Ag nanodisks (565 μl). For further clarification of the quenching property of RhB by Ag nanodisks, the fluorescence quantum yields of RhB with various amounts of Ag nanodisks were calculated and are presented in Table 1. The fluorescence quantum yield of RhB in aqueous solution was 0.35. This value matches the previously reported value.[44] In contrast, the fluorescence quantum yields of RhB with Ag nanodisks showed a significant decrease, depending on the excitation wavelength and the amount of Ag nanodisks. These results strengthen the fact that the fluorescence quenching was correlated with the amount of Ag nanodisks and the excitation wavelength as well. More interestingly, the increase according to the increasing wavelength excitation also was only linear in the range of amount of Ag nanodisks from 130 to 425 μl. The fluorescence quenching mechanism of RhB in the presence of Ag nanodisks will be clarified in the next section.

### 3.4. Fluorescence quenching mechanism of RhB under the influence of Ag nanodisks

It is generally accepted that fluorescence quenching can cause dynamic quenching and/or static quenching. Dynamic quenching is known as the deactivated excited state of fluorophores by quenchers, generally through a collisional mechanism. A significant signature to recognize the dynamic quenching is the decrease in the fluorescence lifetime of fluorophores due to an additional rate process that depopulates the excited state without fluorescence emission. However, statics quenching also causes a decrease in fluorescence intensity, but it shows no changes in the fluorescence lifetime of fluorophores.[15] The fluorescence quenching mechanism based on metal nanomaterials and chlorophores has attracted much research. It is popularly believed that the dynamic quenching mechanism mostly plays an important role in those cases, particularly due to FRET. Seliverstova *et al.* reported the effect of Ag nanoparticles on the fluorescence properties of indopolycarbocyanine dyes with FRET, which acted as a significant factor for changes in the fluorescence intensity.[28] The fluorescence quenching of coumarin dye by silver nanoparticles acting as a quencher was also elucidated due to the FRET mechanism.[26] It was indicated that the FRET mechanism occurred as a result of the spectral overlap of the absorption of silver nanoparticles and emission of coumarin dye.

As a suggestion to evaluate the fluorescence quenching mechanism of RhB in the presence of Ag nanodisks, the absorption and fluorescence spectra of RhB can be compared with the absorption spectrum of Ag nanodisks to compare the relative positions of these spectra (Fig. 7). Fig. 7 shows there was an excellent overlap of Ag nanodisks absorption with both the fluorescence and absorption spectra of RhB. Additionally, as indicated from previous reports, with the presence of Ag nanoparticles, the fluorescence of some dyes (coumarin,[26] rhodamine 6G,[5] RhB[3]) was quenched due to energy transfer between the Ag nanoparticles and dyes.

In our case, we initially considered that the fluorescence quenching of RhB might be expected due to several reasons involving dynamic quenching, IFE, and/or static quenching. To gain a better assessment, the time-resolved fluorescence lifetimes of RhB and the mixtures of RhB and Ag nanodisks were compared. Fig. 8a reveals the fluorescence decays of RhB alone and RhB + Ag nanodisks at two different amounts of stock Ag nanodisks solution in water. The fluorescence decay times of the three solutions were exactly the same. The fluorescence lifetimes of these solutions could be well fitted with a single exponential function. The fluorescence lifetime was 1.63 (±0.01) ns, which corresponded to a radiative rate constant ($k_r$) of 6.13 × $10^8$ ($s^{-1}$). This lifetime indicates a good agreement with the fluorescence lifetime of RhB in aqueous solution.[44,45] Thus, the presence of Ag nanodisks, at either high or low concentrations, had no effect on the fluorescence lifetime of RhB. It is inferred that there were no additional processes that depopulated the excited state of RhB. Therefore, we can rule out the contribution of the dynamic mechanism in fluorescence quenching. This observation differs from most previous studies on silver nanoparticles and dye mixtures, in which energy or electron transfer was reported to play a key role in the fluorescence quenching of fluorophores.[3,26,30] Then, the IFE and/or static quenching are considered the major factors in fluorescence quenching of RhB with Ag nanodisks. Due to the high

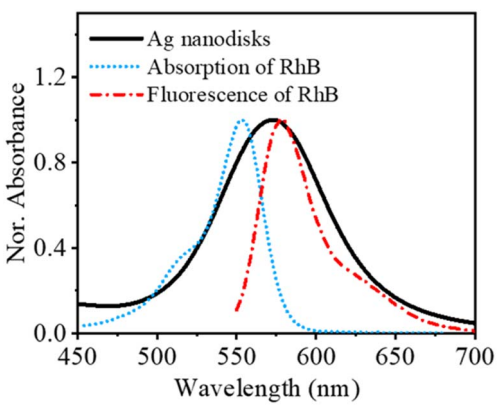


Fig. 7 Spectral overlap of the normalized absorption spectrum of Ag nanodisks (bold black line) in comparison with normalized absorption (short dot line) and fluorescence (dot and dash line) spectra of RhB in aqueous solution.

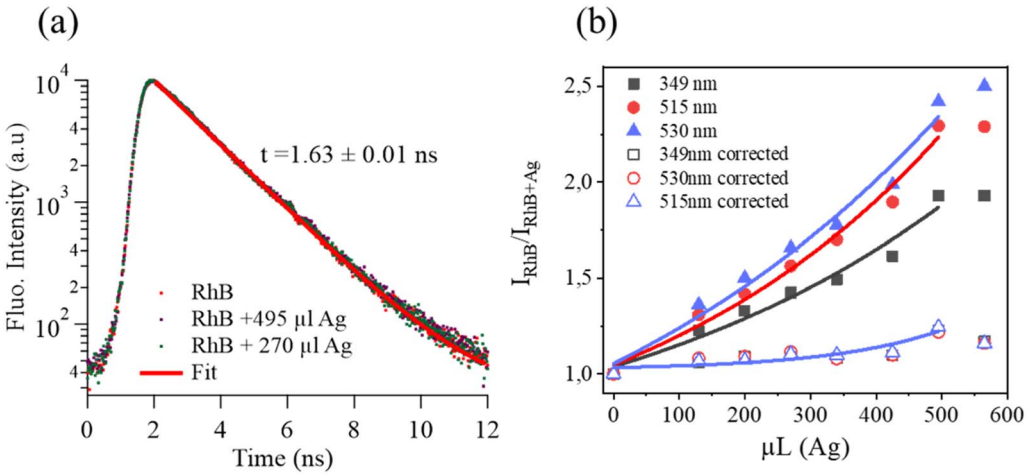


Fig. 8 (a) Time-resolved fluorescence decay of RhB in water with and without Ag nanodisks. $\lambda_{exc}$ = 550 nm, and $\lambda_{em}$ = 577 nm; (b) ratio fluorescence intensity of RhB with and without the various stock Ag nanodisks solution; the solid lines = the fitting curves.

extinction absorption coefficient and complete overlap of the absorption spectrum of Ag nanodisks with the absorption and fluorescence spectra of RhB, the IFE was anticipated to impact RhB fluorescence quenching significantly. First, looking back at examining the fluorescence quenching efficiency under different excitation wavelengths, a clear trend of increasing quenching efficiency corresponding to the increasing excitation wavelength from 349 to 530 nm was obtained (Fig. 6d). Based on the primary IFE, this observation is appropriate and can be explained as follows. The fluorescence intensity is proportional to the fluorophore's quantum yield, the molar extinction coefficient of the fluorophore at the excitation wavelength, and the intensity of the excitation radiation. Then, when the excitation wavelength shifts from 349 to 530 nm, it means that the excitation wavelength shifts to the higher absorption coefficient of RhB, leading to the attenuation of the excitation beam.[13] Furthermore, when the excitation wavelength is shifted from 349 m to 530 nm, this also corresponds to an increase in the ability to reabsorb the excitation radiation and emission radiation of RhB by Ag nanodisks in the solution, known as secondary IFE.[13,15] As a result, the fluorescence intensity of RhB will significantly decrease when increasing the excitation wavelength. In order to quantify the contribution of EFE, the correction for EFE can be calculated as follows:[43,46]

$$\eta = \frac{A_{x0}A_{y0}\left(1-10^{-A_{xi}}\right)\left(1-10^{-A_{yi}}\right)}{A_{xi}A_{yi}\left(1-10^{-A_{x0}}\right)\left(1-10^{-A_{y0}}\right)} \quad (2)$$

where $A_{x0}$ and $A_{y0}$ are the absorbances of the solution of the fluorophore alone (only RhB solution), and $A_{xi}$ and $A_{yi}$ are the absorbances of the mixture solution of the fluorophore and quencher (RhB + Ag nanodisks), at the excitation and emission wavelengths, respectively. The IFE correction was then applied by replacing $I_{RhB}/I_{RhB+Ag}$ with $\eta\, I_{RhB}/I_{RhB+Ag}$. For our case, $\eta$ was estimated for three excitation wavelengths at 349, 515, and 530 nm; while the emission wavelength was taken as 579 nm. As calculated, the $\eta$ values varied from 0.46 (for the case of excitation at 530 nm with the largest amount of Ag nanodisks) to 1 (for the case without Ag nanodisks). After the correction of the IFE contribution, it was revealed that the fluorescence intensity had no dependence on the excitation wavelength, as shown in Fig. 8b (the open symbol curvature); and the ratios of $I_{RhB}/I_{RhB+Ag}$ were approximately 1.1 (±0.02) in the case of the amount of stock solution Ag nanodisks lower than 425 µl. It is thus evident that the IFE plays an important role in the fluorescence quenching of RhB when the presence of Ag nanodisk at the concentration of Ag nanodisks corresponded to the amount of stock Ag nanodisk solution lower than 425 µl. At an amount of stock Ag nanodisks solution larger than 425 µl, the ratio of $I_{RhB}/I_{RhB+Ag}$ was around 1.2 (±0.03). Therefore, except for the contribution of IFE, at higher concentrations of Ag nanodisks, the fluorescence quenching of RhB might be affected by static quenching; this quenching generally occurs at high quencher concentrations.[47]

In the case of static quenching, two distinguished possibilities should be mentioned: (i) the formation of a ground-state non-fluorescent complex, and (ii) the quencher located inside a sphere of effective quenching.[47] For the former case, the absorption spectra of the mixture of Ag nanodisks and RhB simply described the overall Ag nanodisks and RhB without any new band. Therefore, we can ignore the case of the formation of non-fluorescent complexes. To estimate the second possibility of the quencher (Ag nanodisks) located inside or outside a sphere of effective quenching of the fluorophore RhB, the changes in fluorescence intensity depending on the amount of Ag nanodisks need to be evaluated. It is known that if a quencher is outside the active sphere of a fluorophore, it has no effect on the fluorophore.

In contrast, if a quencher is located inside a quenching sphere of a fluorophore, it will lead to its fluorescence quenching. A specific characteristic of the case of fluorescence quenching due to the quencher located inside the active sphere is that the concentration dependence of the quencher *versus* fluorescence intensity is almost linear at low concentrations and shows an upward curvature at high quencher

concentrations.[47] According to Perrin's model, the ratio $I_0/I$ can be expressed by

$$\frac{I_0}{I} = \exp\left(V_q N_a [Q]\right) \quad (3)$$

where $V_q$ is a sphere of volume surrounding the fluorophore, $N_a$ is Avogadro's number, and $[Q]$ is the quencher concentration. At low concentration, $\exp(V_q N_a[Q]) \approx 1 + V_q N_a[Q]$, which is why the concentration dependence was almost linear, similar to the case of the Stern–Volmer plot. In comparison to our case, the dependence of the $I_{RhB}/I_{RhB+Ag}$ ratio on the amount of stock Ag nanodisks well fitted with a growing exponential function (Fig. 8b). Therefore, we inferred that there was a minor contribution of static quenching of RhB in the presence of Ag nanodisks. This contribution was negligible when the amount of Ag nanodisk stock solution was less than 425 μl, and reached about 17% when the amount of Ag stock solution was greater than 475 μl. Silver nanoparticles have been reported to be able to act as acceptors and/or quenchers of fluorophores due to electron transfer and energy transfer.[6,7,26,27,30] For our case, although the spectra overlap between the absorbance (Ag nanodisks) and fluorescence of the fluorophore (RhB) were favorable in terms of fluorescence energy transfer, the fluorescence quenching mechanism of RhB due to triangular silver nanodisks was consistent with the greater contribution of the IFE mechanism. As mentioned above, FRET and/or NEST frequently are predominant contributors to fluorescence quenching due to silver nanomaterials acting as a quencher. The major role of IFE in the fluorescence quenching of RhB was thus unexpected. For suggesting an interpretation, we suppose that the size and shape of Ag nanodisks might be the crucial issue leading to the different quenching mechanisms in comparison to the previous studies based on spherical silver nanomaterial.[5,26,48] It is worth noting that FRET can occur effectively in inverse proportion to the six orders of the center-to-center distance $(1/r^6)$ between dyes and absorbers. Likewise, the interaction between the fluorophore and absorber due to IFE is more predominant at much longer distances, with an $1/r^2$ dependence within the solution.[49] Then, we suppose that the main reason for the significant role of the IFE mechanism in fluorescence quenching stemmed from the interaction distance between the Ag nanodisks and RhB. This interaction is different from the case of silver nanoparticles. In the case of triangular silver nanodisks, it might be due to the shape of the triangular silver nanodisks and the change in charge distribution across their surface.[20] Fluorescence quenching due to the IFE and/or static quenching has also been reported based on some fluorophores, such as carbon nanodots,[17] and azamonardine.[50] Kathiravan *et al.* investigated fluorescence quenching due to the IFE mechanism based on phenothiazine derivatives acting as fluorescence system and picric acid acting as the quencher.[51] Our results provide great guidance for simply designing a high-efficiency fluorescence quenching system for performing fluorescence sensing.

# 4 Conclusions

In summary, we clarified the fluorescence quenching mechanism of a system involving RhB dye and Ag nanodisks in water solutions based on steady-state absorption and fluorescence spectroscopies together with the time-resolved fluorescence lifetime technique. In this system, the Ag nanodisks acted as fluorescent quenchers, leading to quenching of the fluorescence of RhB, mostly due to IFE as the predominant contribution. Additionally, the location of Ag nanodisks inside the sphere of effective quenching of the fluorophore RhB also made a minor contribution to the fluorescence quenching. Interestingly, this study revealed that energy transfer between Ag nanodisks and RhB could not be observed as in most previous studies. This could be due to the size and shape of the triangular silver nanodisks. Our results pave the way to design fluorescence sensing systems, which is a hot and contemporary research theme, with an insight into the fluorescence quenching mechanism.

# Conflicts of interest

There are no conflicts to declare.

# Acknowledgements

This research was supported by the Ministry of Education and Training of Vietnam under grant number B2023-TNA-05 and partially funded by the TNU-University of Sciences under the project code: CS2023-TN06-12.

# References

1 X. Yan, H. Li and X. Su, *TrAC, Trends Anal. Chem.*, 2018, **103**, 1–20.
2 M. I. Gaviria-Arroyave, J. B. Cano and G. A. Peñuela, *Talanta Open*, 2020, **2**, 100006.
3 M. A. M. Torres, A. V. Veglia and N. L. Pacioni, *Microchem. J.*, 2021, **160**, 105645.
4 P. Das, S. Ganguly, S. R. Ahmed, M. Sherazee, S. Margel, A. Gedanken, S. Srinivasan and A. R. Rajabzadeh, *ACS Appl. Polym. Mater.*, 2022, **4**, 9323–9340.
5 G. Rezanejade Bardajee, Z. Hooshyar and M. Khanjari, *J. Photochem. Photobiol., A*, 2014, **276**, 113–121.
6 D. Ghosh and N. Chattopadhyay, *J. Lumin.*, 2015, **160**, 223–232.
7 H. R. Deepa, S. Chandrasekhar and J. Thipperudrappa, *Chem. Phys. Impact*, 2022, **4**, 100075.
8 C. Chen and N. Hildebrandt, *TrAC, Trends Anal. Chem.*, 2020, **123**, 115748.
9 G. Chen, F. Song, X. Xiong and X. Peng, *Ind. Eng. Chem. Res.*, 2013, **52**, 11228–11245.
10 C. Xu, Y. Zhou, Y. Zhou, Z. Li and X. Peng, *Sens. Actuators, B*, 2020, **325**, 128766.
11 S. Chen, Y. L. Yu and J. H. Wang, *Anal. Chim. Acta*, 2018, **999**, 13–26.
12 P. Yuan and D. R. Walt, *Anal. Chem.*, 1987, **59**, 2391–2394.
13 S. Kumar Panigrahi and A. Kumar Mishra, *J. Photochem. Photobiol., C*, 2019, **41**, 100318.
14 M. Zhang, X. Cao, H. Li, F. Guan, J. Guo, F. Shen, Y. Luo, C. Sun and L. Zhang, *Food Chem.*, 2012, **135**, 1894–1900.

15 J. R. Lakowicz, *Principles of Fluorescence Spectroscopy*, Springer, 2006.
16 H. Fan, G. Q. Xiang, Y. Wang, H. Zhang, K. Ning, J. Duan, L. He, X. Jiang and W. Zhao, *Spectrochim. Acta, Part A*, 2018, **205**, 221–226.
17 B. R. Al-Hashimi, K. M. Omer, H. S. Rahman and H. H. Othman, *Spectrochim. Acta, Part A*, 2021, **244**, 118835.
18 P. Das, M. Sherazee, P. K. Marvi, S. R. Ahmed, A. Gedanken, S. Srinivasan and A. R. Rajabzadeh, *ACS Appl. Mater. Interfaces*, 2023, **15**(24), 29425–29439.
19 L. Ding, H. Yang, S. Ge and J. Yu, *Spectrochim. Acta, Part A*, 2018, **193**, 305–309.
20 K. L. Kelly, E. Coronado, L. L. Zhao and G. C. Schatz, *J. Phys. Chem. B*, 2003, **107**, 668–677.
21 D. E. Charles, D. Aherne, M. Gara, D. M. Ledwith, Y. K. Gun'ko, J. M. Kelly, W. J. Blau and M. E. Brennan-Fournet, *ACS Nano*, 2010, **4**, 55–64.
22 W. Yu, X. Lin, N. Duan, Z. Wang and S. Wu, *Anal. Chim. Acta*, 2023, **1244**, 340846.
23 N. Li, L. Shi, X. Zou, T. Wang, D. Wang, Z. Gong and M. Fan, *Microchem. J.*, 2022, **173**, 107046.
24 H. Chen, L. Zhang, Y. Hu, C. Zhou, W. Lan, H. Fu and Y. She, *Sens. Actuators, B*, 2021, **329**, 129135.
25 A. Moores and F. Goettmann, *New J. Chem.*, 2006, **30**, 1121–1132.
26 V. V. Koppal, P. G. Patil, R. M. Melavanki, R. A. Kusanur, U. O. Afi and N. R. Patil, *J. Mol. Liq.*, 2019, **292**, 111419.
27 V. V. Koppal, R. M. Melavanki, R. A. Kusanur and N. R. Patil, *J. Mol. Liq.*, 2018, **269**, 381–386.
28 E. Seliverstova, N. Ibrayev, G. Omarova, A. Ishchenko and M. Kucherenko, *J. Lumin.*, 2021, **235**, 118000.
29 S. Saini, V. B. Shenoy and B. Bagchi, *J. Phys. Chem. C*, 2008, **112**, 6299–6306.
30 D. S. Rahman, S. Deb and S. K. Ghosh, *J. Phys. Chem. C*, 2015, **119**, 27145–27155.
31 J. E. Millstone, S. J. Hurst, G. S. Métraux, J. I. Cutler and C. A. Mirkin, *Small*, 2009, **5**, 646–664.
32 R. Pagano, M. Ottolini, L. Valli, S. Bettini and G. Giancane, *Colloids Surf., A*, 2021, **624**, 126787.
33 K. L. Shuford, M. A. Ratner and G. C. Schatz, *J. Chem. Phys.*, 2005, **123**, 114713.
34 S.-W. Lee, S.-H. Chang, Y.-S. Lai, C.-C. Lin, C.-M. Tsai, Y.-C. Lee, J.-C. Chen and C.-L. Huang, *Materials*, 2014, **7**, 7781–7798.
35 R. F. Kubin and A. N. Fletcher, *J. Lumin.*, 1982, **27**, 455–462.
36 S. Farooq, F. Dias Nunes and R. E. de Araujo, *Photonics Nanostructures: Fundam. Appl.*, 2018, **31**, 160–167.
37 S. Mukherji, S. Bharti, G. Shukla and S. Mukherji, *Phys. Sci. Rev.*, 2019, **4**, 20170082.
38 X. H. Vu, N. D. Dien, T. T. Ha Pham, T. T. Trang, N. X. Ca, P. T. Tho, N. D. Vinh and P. Van Do, *RSC Adv.*, 2020, **10**, 38974–38988.
39 T. T. Tran, X. H. Vu, T. L. Ngo, T. T. H. Pham, D. D. Nguyen and V. D. Nguyen, *Phys. Chem. Chem. Phys.*, 2023, **25**, 15941–15952.
40 T. T. Ha Pham, X. H. Vu, N. D. Dien, T. T. Trang, N. Van Truong, T. D. Thanh, P. M. Tan and N. X. Ca, *RSC Adv.*, 2020, **10**, 24577–24594.
41 S. T. Gentry, S. F. Kendra and M. W. Bezpalko, *J. Phys. Chem. C*, 2011, **115**, 12736–12741.
42 Y. Zao, J.-b. ZHANG, H. Hua, X.-b. XU, B.-c. LUO, X.-b. LI, L. Kai, N. Gao, X.-l. TAN and J.-s. LUO, *Trans. Nonferrous Met. Soc. China*, 2012, **22**, 865–872.
43 S. A. Raza, S. Q. Naqvi, A. Usman, J. R. Jennings and Y. W. Soon, *J. Photochem. Photobiol., A*, 2021, **418**, 113417.
44 X.-F. Zhang, Y. Zhang and L. Liu, *J. Lumin.*, 2014, **145**, 448–453.
45 M. Snare, F. Treloar, K. Ghiggino and P. Thistlethwaite, *J. Photochem.*, 1982, **18**, 335–346.
46 I. E. Borissevitch, *J. Lumin.*, 1999, **81**, 219–224.
47 B. Valeur and M. N. Berberan-Santos, *Molecular Fluorescence: Principles and Applications*, John Wiley & Sons, 2012.
48 H. R. Deepa, H. M. S. Kumar, M. Basanagouda and J. Thipperudrappa, *Can. J. Phys.*, 2014, **92**, 163–167.
49 Y. Li, R. Su, H. Li, J. Guo, N. Hildebrandt and C. Sun, *Anal. Chem.*, 2021, **94**, 193–224.
50 L. Chen, C.-P. Du, L. Qi, Y. Wang, K.-L. Pei, R.-W. Zhang and W.-J. Qi, *Chin. J. Anal. Chem.*, 2022, **50**, 100165.
51 A. Kathiravan, M. Narayanan, M. Asha Jhonsi and V. Anbazhagan, *Spectrochim. Acta, Part A*, 2023, **303**, 123166.